MANUFACTURED NANOPARTICLES: POTENTIALLY TOXIC AGENTS OR NUTRIENT RESERVOIRS FOR PLANTS?

Zoltán Klencsár[1], Krisztina Kovács[2], Ferenc Fodor[3], Ádám Solti[3], Gyula Tolnai[1], Zoltán Sándor[1], Zoltán May[1], Ervin Gy. Szabó[1], Péter Németh[1], László Szabó[1], Fruzsina Pankaczi[3], Zita Fülöp[3], Zsuzsanna Farkas[3], Zoltán Homonnay[2], Ernő Kuzmann[2]

[1]*Institute of Materials and Environmental Chemistry, Research Centre for Natural Sciences, Hungarian Academy of Sciences, Magyar tudósok körútja 2, 1117 Budapest, Hungary*

[2]*Institute of Chemistry, Eötvös Loránd University, Pázmány P. s. 1/A, 1117 Budapest, Hungary*

[3]*Institute of Biology, Eötvös Loránd University, Pázmány P. s. 1/A, 1117 Budapest, Hungary*

1. Introduction

The magnitude and importance of production and industrial utilization of **manufactured nanoparticles (MNPs)** has been increasing rapidly in recent years [1]. According to estimates [2], the total worldwide production of nanomaterials exceeded the order of 10^5 t/year already in 2012. It is quite plausible that a considerable fraction of the produced nanoparticles will finally find its way from the industry and consumer products to different environmental compartments such as air, water and soil [3]. Despite growing concerns regarding the **environmental risks of MNPs**, as of today, knowledge about their transport, possible transformations, final fate and concentration in the ecosystems is scarce [3]. Even more alarming is the lack of comprehensive knowledge and understanding of the nature and mechanisms of the effects of MNPs on their possible host ecosystems and the associated living organisms such as algae, plants, and fungi, which are expected to be affected by an exposure to MNPs [4].

Plants may be exposed to MNPs in the atmosphere (through leaves) as well as in the soil (via roots). Airborne MNPs may directly enter plants through stomata and bases of trichomes, as well as they may lead to the obstruction of stomata with associated alteration of the leaves' gas exchange and thus photosynthesis. A direct physical interaction between the roots and MNPs polluting the soil may take place via endocytosis during the growth of root hair cells. **Nanoparticles with a diameter less than about 20 nm may also pass through the plant cell wall and reach the plasma membrane of plant cells.** Direct chemical interaction can take place between nanoparticles and root secretions in the rhizosphere, where—prior to potential uptake by the plant—metals can participate in chemical reactions leading to their solubilization via reduction and/or chelation.

Suitable **MNPs** may also serve **as nutrient reservoirs** in their host ecosystem. For high quality and efficient crop production, it is inevitable to ensure optimal nutrition for the plants: in case of low-quality soil (such as those with high soil pH), missing nutrients should be supplied by appropriate fertilizers. Insufficient supply of **Fe**, for example, hampers chlorophyll biosynthesis, leading to slow growth, low plant biomass and nutrition value (Figure 1). Controlled exposure to selected iron-containing nanoparticles **may** therefore also turn out to **be beneficial to ecosystems** involving plants.

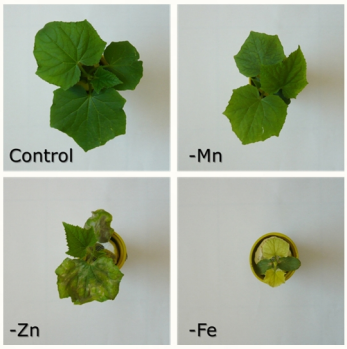

Figure 1. Illustration of the effect of insufficient manganese, zinc and iron supply on the development of cucumber plant, in comparison with a control plant grown under normal conditions. The indicated micronutrient deficiencies were maintained in hydroponics for a 3-weeks growth period.

In addition to iron, in calcareous and alkaline soils micronutrient constraints related especially to Mn and Zn are regarded as the most serious nutritional problems for plants [5]. While **Mn** plays a key role in photosynthesis by forming the Mn_4CaO_5 core of the manganese-calcium water-oxidizing complex of photosystem II, **Zn** is involved in plant photosynthesis in the form of a metalloenzyme that catalyzes the inter-conversion of CO_2 and H_2O into HCO_3^- ions [6]. Insufficient supply of these micronutrients can thus also lead to a pathological state and hindered development of plants (Figure 1).

MNPs incorporating Fe, Mn and Zn are therefore promising candidates for being used in metal biofortification of plants.

In this work **we aim to explore the effects of iron-based nanoparticles on plants** of cucumber (Cucumis sativus) via controlled plant-growth experiments. We introduce results related to Fe-Co alloy, ferric-oxide-hydroxide and MnZn-ferrite nanoparticles.

4. Plant growth experiments

In **toxicity experiments** 12-days administration of 0.1 mM iron-equivalent **Fe-Co alloy nanoparticles** to healthy plants **led to a pathological plant state** with symptoms akin to those of iron deficiency chlorosis: strongly hindered growth leading to low biomass and low chlorophyll levels leading to yellowish leaves. Tenfold increase in the Fe-Co alloy concentration further amplified the deterioration of the plant that could hardly develop in comparison with a healthy control. Administration of Fe-Co resulted in extreme high cobalt concentration and decreased Fe concentration levels in the plants (Figure 11), indicating that the observed pathological plant state developed due to **cobalt poisoning**. With respect to the control (with ~2 mg Chl/g fresh weight), in the Fe-Co treated plants chlorophyll concentration levels got reduced by an order of magnitude, the reduction being more pronounced when higher (1 mM) concentration of Fe-Co was applied.

In **regeneration experiments** the FH1 and MZF colloid suspensions were found to be an efficient iron source for iron deficient cucumber plants (Figures 12, 13). Plants grown under Fe-deficient conditions for 2 weeks recovered due to 1 week 0.01 mM FH1 administration by reaching iron concentration levels equal to or higher than that of the control.

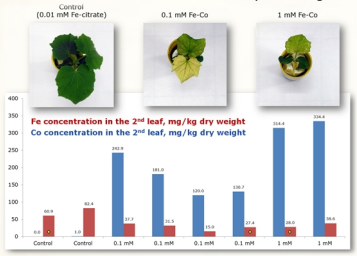

Figure 11. Effect of 12-days long Fe-Co alloy administration on the development of cucumber plants (previously grown on 0.01 mM Fe-citrate for 9 days) in comparison with healthy control grown continuously on 0.01 mM Fe-citrate. Photos illustrate typical results, whereas the 2nd leaf's resulting Fe and Co concentration levels (from **ICP-OES**) are shown as bars for different Fe-Co concentrations underneath.

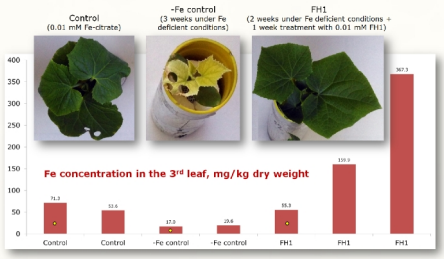

Figure 12. Effect of 1-week long FH1 colloid suspension sample administration on the development of cucumber plants (previously grown under Fe-deficient conditions for 2 weeks) in comparison with healthy control grown continuously on 0.01 mM Fe-citrate, and -Fe control that was continuously grown under Fe-deficient conditions. Typical results are illustrated as photos on the top, whereas the 3rd leaf's resulting Fe concentration levels determined via **ICP-OES** measurements in individual cases are shown as bars underneath.

X-band EPR spectroscopy of dried leaves of the plants revealed three distinct signals with $g \approx 2$: a narrow ($\Gamma_{pp} \approx 7$ G) singlet (**A**) at $g \approx 2.002(1)$ that may originate from semiquinone type free radicals formed via the oxidation of polyphenolic plant compounds, a broadened sextet component (**B**) related to presumably protein-bound, high-spin Mn^{2+} species, and a broad ($\Gamma_{pp} \approx 500$ G) underlying peak (**C**) from exchange-coupled transition metals, presumably mainly Fe. The specific intensity of peak **A** was found to correlate with the chlorophyll concentration of leaves with a linear correlation coefficient of $r \approx +0.9$, leaves of healthier plants tending to exhibit an **A** signal with larger specific intensity (Figure 13).

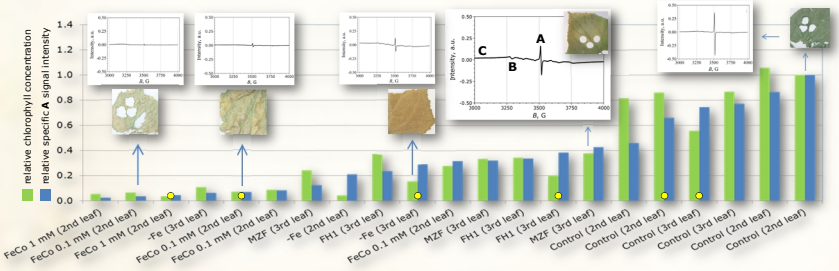

Figure 13. Relative chlorophyll concentration and relative specific **A** EPR signal intensity of selected dried leaves of cucumber plant samples. Photos of the dried leaves (illustrating the apparent health status of the source plants) and corresponding X-band EPR spectra are given for selected examples. Yellow dots denote cases corresponding to similarly marked experiments on Figures 11 and 12. **FeCo** denotes results of toxicity experiments. Cases marked with **FH1** and **MZF** refer to results of corresponding regeneration experiments. **–Fe** denotes cases where the plant was grown exclusively on iron deficient conditions. Cases designated as **Control** refer here to healthy plants.

5. Conclusions

Our results underline the possibility of interactions between plants and nanoparticles by revealing that iron(III) oxide-hydroxide, MnZn-ferrite and Fe-Co alloy nanoparticles are all able to influence the quality and productivity of cucumber plants grown in hydroponics, the effects being essentially favorable in case of iron(III) oxide-hydroxide and MnZn-ferrite, and essentially toxic when Fe-Co alloy nanoparticles are administered to the plant.

Acknowledgement. Financial support from the National Research, Development and Innovation Office - NKFIH/OTKA (K115913 and K115784) is gratefully acknowledged.

2. Experimental

As reliable knowledge concerning the effects of nanoparticles on plants can only be gained if the nanoparticle agent being subject of the study is properly characterized for its relevant physico-chemical attributes, it is inevitable that plant growth experiments are supported with materials science providing in-depth characterization of the nanoparticles and the plants alike. We aim to achieve this by applying a wide range of experimental techniques—including XRD, TEM, ICP-MS/OES, EPR/FMR and ^{57}Fe Mössbauer spectroscopy (^{57}Fe MS) as well as chlorophyll concentration measurements—in order to assess the attributes of the prepared nanoparticles and those of the plant samples. The experiments were carried out by the following equipments. Philips PW3710 based PW1050 Bragg-Brentano goniometer system used with Cu Kα radiation along with graphite monochromator (XRD), Morgagni 268D (100 kV) transmission electron microscope (TEM), Thermo Scientific "iCAP Qc" (ICP-MS) and Spectro Genesis (ICP-OES) spectrometers, Bruker ElexSys E500 X-band spectrometer (EPR/FMR), WISSEL spectrometer applied in transmission geometry along with a source of ^{57}Co in Rh matrix providing the γ-rays with ca. 20 mCi activity (^{57}Fe MS).

Fe-Co alloy nanoparticles were prepared via wet chemical synthesis, by using iron(III) chloride hexahydrate and cobalt(II) acetate as precursors with aluminium powder and ammonium fluoride applied as reducing materials as described in [7]. Stable **colloid suspension of iron(III)-oxihydroxide nanoparticles** (**FH1**) was prepared via wet chemical synthesis with a concentration of ~ 0.37 mg/cm^3 for the colloidal fractions. The corresponding iron concentration was estimated to be ~ 0.26 mg/cm^3 [8]. For the XRD measurement a powder sample (**FH2**) was prepared from an analogous colloid suspension. **$Mn_{0.25}Zn_{0.75}Fe_2O_4$ colloid suspension** (sample **MZF**, colloid concentration 35.6 mg/cm^3) was prepared via sol-gel hydrothermal process starting from a mixed solution of Mn^{2+}, Zn^{2+} and Fe^{3+} salts in strongly alkaline aqueous medium as described in [9].

Plant growth experiments were carried out in hydroponics. In the case of Fe-Co alloy nanoparticles the experiments aimed at the exploration of **potentially toxic effects** that may be expected on account of the known phytotoxic nature of Co [10]. Accordingly, the alloy was administered to healthy plants in high concentrations (including either 0.1 mM or 1 mM of Fe) for a 12-days period. In contrast, the FH1 and MZF colloid suspensions were administered to iron deficient plants in lower concentrations (including 0.01 mM of iron) for a 1-week period in order to explore whether the plant can make use of the nanoparticles in a way that leads to its **regeneration**. After the treatments the health status of the plants was quantified by measuring the chlorophyll concentration in their leaves.

3. Characterization of nanoparticles

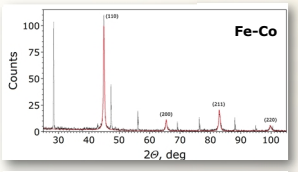

Figure 2. Cu Kα powder **X-ray diffractogram** of the **Fe-Co alloy** nanoparticles used in the plant growth experiments. Reflections belonging to the bcc alloy phase are marked with corresponding Miller indices and the outline of the fitting curve. Most narrow peaks belong to Si powder deliberately added to the sample for calibration purposes. The small peak at $2\Theta \approx 43$ deg may belong to the minor ferric-oxide-hydroxide phase that shows up as a small doublet in the corresponding ^{57}Fe Mössbauer spectrum (Figure 3). Analysis of the diffractogram leads to a cubic lattice parameter of $a \approx 0.2850$ nm and a mean crystallite size of $d \approx 36$ nm, in good agreement with our previous results [7], which confirms the successful preparation of the Fe-Co alloy nanoparticles.

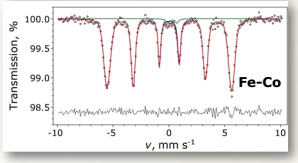

Figure 3. Room-temperature **^{57}Fe Mössbauer spectrum** of the **Fe-Co alloy** nanoparticles used in the plant growth experiments. The spectrum clearly reflects the presence of Fe-Co alloy in the form of a major sextet component displaying pronounced line broadening due to the presence of a large variety of iron atomic environments. The latter evidences a random distribution of Fe and Co atoms over the α and β sites of the bcc lattice in agreement with our previous results [7]. A small doublet component refers to the presence of a ferric-oxide-hydroxide minority phase that is a side product of the preparation procedure [7]. A fit of the sextet component to a model assuming binomial probability distribution of the number of iron atoms as nearest and next-nearest neighbor to a selected iron atom leads to an iron concentration of 56(3)%, confirming a nearly equiatomic alloy composition of ca. $Fe_{0.56}Co_{0.44}$.

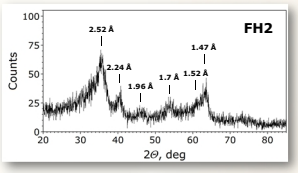

Figure 4. Cu Kα powder **X-ray diffractogram** of the **FH2** ferric-oxide-hydroxide sample. The indicated six broad reflections are a clear fingerprint of 6-line ferrihydrite, a poorly crystalline ferric-oxide-hydroxide [8,11]. The interplanar distances indicated for the associated peaks are in good agreement with literature data [11]. The width of the reflections is consistent with a crystallite size of 4-5 nm. There is a shoulder of the most intense peak at $2\theta \approx 33$ deg that may refer to the presence of extremely small (~ 1-2 nm) hematite nanoparticles in the sample [11].

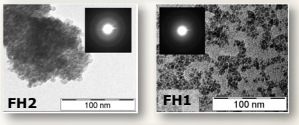

Figure 5. TEM images of the **FH2** and **FH1** ferric-oxide-hydroxide samples, with the corresponding electron diffraction patterns shown as insets. The characteristic particle size is ~ 5 nm in both cases, in good agreement with the crystallite size observed for FH2 (Figure 4). The structure of characteristic interplanar distances reflected by the electron diffraction patterns corresponds well to that of the XRD reflections of FH2 (Figure 4), and thereby indicates that particles in the FH1 colloid suspension have a structure similar to that of particles in the powder FH2.

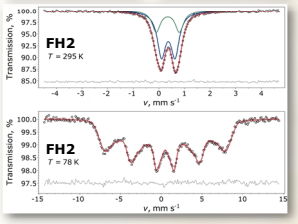

Figure 6. ^{57}Fe Mössbauer spectrum of the FH2 ferric-oxide-hydroxide powder sample at room temperature (top) and at 78 K (bottom). The RT spectrum can be decomposed into two Lorentzian doublets with parameters ($\delta_1 = 0.37$ mm/s, $\Delta_1 = 0.53$ mm/s, $\delta_2 = 0.9$ mm/s) and a spectral area ratio (~2:1) close to the corresponding parameters of β-FeOOH (akaganéite) [12], which confirms that iron atoms in the FH2 nanoparticles have atomic environments corresponding to those expected to occur in ferric-oxide-hydroxide. At the same time, the obtained parameters are also akin to those reported in [13] for a well-crystallized ferrihydrite sample. The spectrum at 78 K displays magnetic splitting with a wide hyperfine magnetic field distribution that can be fitted well with the method of Hesse and Rübartsch even without the assumption of hyperfine parameter correlations. The isomer shift is $\delta \approx 0.50(1)$ mm/s at 78 K. The quadrupole shift was assumed to be zero in the shown fit, when it is allowed to change it takes on a value corresponding to $2\varepsilon \approx -0.08(2)$ mm/s. The hyperfine magnetic field distribution takes on its maximum value at ~ 46 T.

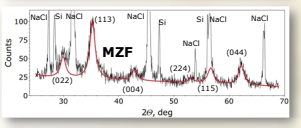

Figure 7. Cu Kα **X-ray diffractogram** of a powder sample obtained by drying a portion of the **MZF** ($Mn_{0.25}Zn_{0.75}Fe_2O_4$) colloid suspension. Reflections belonging to the cubic spinel ferrite are marked with the corresponding Miller indices and the outline of the fitting curve. Part of the narrow reflections (some of them not fully displayed for the sake of the better visibility of the small-intensity ferrite peaks) belongs to Si powder deliberately added to the sample for calibration purposes, while the remaining part belongs to cubic NaCl crystals being a side product of the preparation procedure. A fit provides a cubic lattice parameter of $a = 0.8439(2)$ nm and a mean crystallite size of $d \approx 8$ nm for the ferrite sample.

Figure 8. TEM image of the **MZF** ($Mn_{0.25}Zn_{0.75}Fe_2O_4$) colloid suspension sample. The characteristic particle size range of the ferrite is ca. 5-10 nm, in good agreement with the crystallite size observed for the corresponding powder sample (Figure 7).

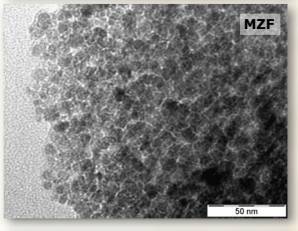

Figure 9. X-band EPR spectrum (derivative of the microwave absorption versus the applied magnetic field) of the **MZF** colloid suspension sample (measured in capillary, at room temperature). The narrow peak near $g = 2$ corroborates the superparamagnetic nature of the nanoparticles in accordance with the small particle size [9].

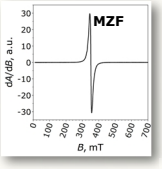

Figure 10. ^{57}Fe Mössbauer spectrum of a $Mn_{0.25}Zn_{0.75}Fe_2O_4$ powder sample [9] prepared analogously to **MZF**. The doublet is characterized with broad ($W_1 \approx 0.87$ mm/s) absorption peaks and a minor shoulder that refer to the role of magnetic relaxation phenomena in determining the spectral shape. The blocking temperature is clearly below 140 K, which is consistent with the small particle size observed for the analogous sample MZF. Note that the magnetic ordering temperature of this sample was previously estimated to be ~ 360 K [9]. A fit to a quadrupole doublet of Lorentzian lines leads to hyperfine parameters of $\delta \approx 0.43$ mm/s and $\Delta \approx 0.6$ mm/s.

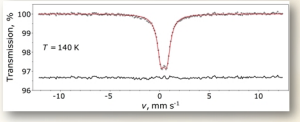

References

[1] A. Bour, F. Mouchet, J. Silvestre, L. Gauthier, E. Pinelli: *J. Hazardous Materials* **283** (2015) 764.
[2] F. Piccinno, F. Gottschalk, S. Seeger, B. Nowack: *J. Nanopart. Res.* **14** (2012) 1109.
[3] J.D. Posner: *Nano Today* **4** (2009) 114.
[4] E. Navarro, A. Baun, R. Behra, N.B. Hartmann, J. Filser, A. Miao, A. Quigg, P.H. Santschi, L. Sigg: *Ecotoxicology* **17** (2008) 372.
[5] T. Chatzistathis: *Plant Responses to Iron, Manganese, and Zinc Deficiency Stress*, in P. Ahmad, S. Rasool (editors): Emerging Technologies and Management of Crop Stress Tolerance (Academic Press, 2014), Volume 1: Biological Techniques, Chapter 13, pp. 293–311.
[6] I. Yruela: *Metallomics* **5** (2013) 1090.
[7] Z. Klencsár, P. Németh, Z. Sándor, T. Horváth, I.E. Sajó, S. Mészáros, J. Mantilla, J.A.H. Coaquira, V.K. Garg, E. Kuzmann, Gy. Tolnai: *J. Alloys and Compounds* **674** (2016) 153.
[8] Z. Homonnay, Gy. Tolnai, F. Fodor, Á. Solti, K. Kovács, E. Kuzmann, A. Ábrahám, E.Gy. Szabó, P. Németh, L. Szabó, Z.Klencsár: *Hyperfine Interactions* **237** (2016) 127.
[9] Z. Klencsár, Gy. Tolnai, L. Korecz, I. Sajó, P. Németh, J. Osán, S. Mészáros, E. Kuzmann: *Solid State Sciences* **24** (2013) 90.
[10] W.B. Hanna, S. Cheng, W.D. McElroy: *Archives of Biochemistry and Biophysics* **54** (1955) 206.
[11] D. Carta, M.F. Casula, A. Corrias, A. Falqui, G. Navarra, G. Pinna: *Mat. Chem. Phys.* **113** (2009) 349.
[12] E. Murad: *Clay Minerals* **14** (1979) 273–283.
[13] E. Murad: *Journal of Magnetism and Magnetic Materials* **74** (1988) 153.